Biosensors and Bioelectronics 135 (2019) 208–215

Contents lists available at ScienceDirect

Biosensors and Bioelectronics

journal homepage: www.elsevier.com/locate/bios

A ratiometric fluorescence platform based on boric-acid-functional Eu-MOF for sensitive detection of H_2O_2 and glucose☆

Yu Cui[a], Fei Chen[a], Xue-Bo Yin[a,b,*]

[a] State Key Laboratory of Medicinal Chemical Biology and Tianjin Key Laboratory of Biosensing and Molecular Recognition, College of Chemistry, Nankai University, Tianjin, 300071, China

[b] Collaborative Innovation Center of Chemical Science and Engineering (Tianjin), Nankai University, Tianjin, 300071, China

ARTICLE INFO

Keywords:
Ratiometric detection
Boric acid group
Eu-MOF
H_2O_2
Glucose

ABSTRACT

A Eu-metal organic framework (Eu-MOF) probe with dual-emission was reported for the ratiometric fluorescence detection of H_2O_2 and glucose. Because of the special nucleophilic reaction between boric group and H_2O_2, Eu^{3+} and 5-boronobenzene-1,3-dicarboxylic acid (BBDC) were selected to synthesize the functional MOF probe via a simple one-pot solvothermal method. The Eu-MOF shows dual-emission at 370 and 623 nm with the single excitation at 270 nm due to the energy transfer efficiency change for antenna effect procedure. After addition of H_2O_2, the red emission of Eu-MOF weakened and the blue emission enhances immediately under 270 nm irradiation, so the ratiometric fluorescence detection is established. Moreover, the obvious color change for visual measuring of H_2O_2 and glucose is illustrated to reveal the merit of Eu-MOF probe. The proposed method was demonstrated to be highly sensitive and selective for H_2O_2 and glucose, with the low detection limits of 0.0335 and 0.0643 μM, respectively. The established boric-acid-functional Eu-MOF sensing platform was proved as the powerful probe for H_2O_2 and the metabolites involved in H_2O_2-generating reaction.

1. Introduction

Hydrogen peroxide (H_2O_2) is one of reactive oxygen species (ROS) and an essential participant in energy (Jiang et al., 2018), food (Zhang et al., 2018a), electrochemistry (Zhu et al., 2017), enzyme catalysis (Chang et al., 2017), and environmental detection (Jia et al., 2018). Moreover, H_2O_2 is an effective biomarker of several cellular processes, including protein folding, growth, signaling, differentiation, and migration in the cells (Foreman et al., 2003; Srikun et al., 2011; Paulsen and Carroll, 2013). Aberrant accumulation of H_2O_2 resulted in oxidative stress and the level of H_2O_2 was also connected to aging and some serious diseases, including diabetes, cardiovascular disorder, cancer, and Alzheimer (Lin and Beal, 2006; Hansson and Libby, 2006). Therefore, H_2O_2 plays an important role as a signaling molecule in monitoring human health and life and it is urgent and necessary to develop a rapid and sensitive H_2O_2 detection strategy for earlier catching and treating (Nosaka and Nosaka, 2017; Gough and Cotter, 2011).

Metal organic frameworks (MOFs) have drawn increased attention in recent years due to their tunable pore size, diverse structure, and abundant functional design (Yaghi et al., 2003; Furukawa et al., 2013). Lanthanide metal organic frameworks (Ln-MOFs) own more particular luminescent properties, such as large Stokes shift, high quantum yields, long decay lifetime and undisturbed emissive energy (Hu et al., 2014; Wang et al., 2018a,b; Yan, 2017; Xue et al., 2018), especially for Tb (III)-MOFs and Eu(III)-MOFs (Liu et al., 2016; Cui et al., 2012). The Ln-MOFs have been recognized as potential fluorescent probes because of their wide emission from blue to infrared (Gallis et al., 2017). Majority of Ln-MOF probes were designed and used with the single emission from lanthanide ions, which were sensitized by ligands based on antenna effect procedure (Dong et al., 2016; Zhang et al., 2018b; Sun et al., 2017; Zhou et al., 2014). While the intensity of single emission fluorescence is often interrupted by the concentration and environment of probes, dual-fluorescence emission provides built-in correction for ratiometric detection and a large color difference easy-to-differentiate with naked eye (Lee et al., 2015). Together, high sensitive and selective probes with dual-fluorescence are critically required to be designed with lanthanide ions and appropriate ligands, and thus dual-emission can be expected from the sensitized lanthanide ions and the ligand itself under single excitation.

☆ Dedicated to the 100th anniversary of Nankai University.

* Corresponding author. State Key Laboratory of Medicinal Chemical Biology and Tianjin Key Laboratory of Biosensing and Molecular Recognition, College of Chemistry, Nankai University, Tianjin, 300071, China.

E-mail address: xbyin@nankai.edu.cn (X.-B. Yin).

https://doi.org/10.1016/j.bios.2019.04.008
Received 25 November 2018; Received in revised form 15 March 2019; Accepted 4 April 2019
Available online 10 April 2019
0956-5663/

Boric acid is a typical functional group which is used to recognize H_2O_2 and glycol (Dickinson and Chang, 2008; Van de Bittner et al., 2010; Sun et al., 2013; Carroll et al., 2014). Simultaneously, boric acid could tune the energy level of the ligand because of its electron-deficient properties. Therefore, dual fluorescence emission from single excitation could be realized for boric-acid-functional Ln-MOFs. The dual-fluorescence emission Eu-MOF prepared with 5-boronobenzene-1,3-dicarboxylic acid (BBDC) as a ligand have been successfully used for sensing F^- (Yang et al., 2017). Considering that F^- ions and H_2O_2 do not often coexist in the same sample and therefore the interaction between boric acid group and H_2O_2 is rarely interfered from F^- ions. A sensitive H_2O_2 probe based on the Eu-MOF was assumed feasible. Although the detection of H_2O_2 using different methods, such as chemiluminescence (Cowan et al., 2013; Chen et al., 2018), electrochemistry (Peng et al., 2018; Zhang et al., 2017), and absorption spectroscopy (Fang et al., 2018), has been developed, ratiometric fluorescence sensing with Ln-MOFs has not been reported yet.

Herein, we optimized experimental factors and successfully synthesized the Eu-MOF hollow spheres with Eu^{3+} as metal node and BBDC as ligand. With the introduction of boric acid as functional group, Eu-MOF exhibits dual emission at 370 and 623 nm, respectively, similar to the corresponding emission from BBDC and Eu^{3+} ions. All the two steady state emissions were recorded under the single excitation at 270 nm. When H_2O_2 was added, the efficiency of the energy transfer from BBDC to Eu^{3+} ions decreased because of the interaction between boric acid group and H_2O_2. Therefore, easy and rapid visible color change occurred from bright red into blue. A low detection limit and high selectivity were achieved for H_2O_2 detection with the Eu-MOF as probe. As a contrast, Tb-MOF was prepared with Tb^{3+} and BBDC and used to reveal the response mechanism and the efficiency of Eu-MOF. Compared with the single fluorescence intensity change of the Tb-MOF probe with green luminescence, the Eu-MOF we designed is easier to distinguish with color change by naked eye for the detection of H_2O_2. Since glucose can be catalyzed to produce H_2O_2 by glucose oxidase (GOx), the Eu-MOF is also an appropriate probe for glucose detection. This strategy overcomes the low sensitivity of the direct detection through boric acid-saccharide interaction because of the lack of sufficient electronic changes (James et al., 1995). The results validated that boric-acid-functional Eu-MOF is promising to sensitively and selectively detect H_2O_2 and glucose in environment and personal health.

2. Materials and methods

2.1. Reagents and chemicals

Europium (III) chloride hexahydrate ($EuCl_3{\cdot}6H_2O$), terbium (III) chloride hexahydrate ($TbCl_3{\cdot}6H_2O$) was obtained from Sigma − Aldrich (Shanghai, China). 5-boronobenzene-1, 3-dicarboxylic acid (BBDC) was purchased from HWRK Chemicals Co., Ltd. (Beijing, China). Hydrogen peroxide (H_2O_2) was obtained from Aladdin BioChem Technology Co., Ltd. (Shanghai, China). Glucose was obtained from Cambridge Isotope Laboratories, Inc.. Glucose oxidase (GOx, 10000 GODU/g) was obtained from Yuanye Biological Co., Ltd. (Shanghai, China). All the chemicals were at least of analytical grade and used as received without further purification. Ultrapure water was purified with an Aquapro system (18.25 MΩ cm) in all the work.

2.2. Instrumentation and characterization

Steady-state fluorescence were recorded on a Hitachi Model FL-4500 fluorescence spectrometer. FTIR spectroscopy (Bruker, Model TENSOR 27) was used ($400-4000\ cm^{-1}$) for Fourier transform infrared (FT-IR) spectra (KBr pellet). Powder X-ray diffraction (PXRD) patterns were carried out on a Model D/max-2500 X-ray diffractometer (Rigaku, Japan) with Cu Kα radiation (λ = 1.5418 Å) at 298 K. High-resolution transmission electron microscopy (HRTEM) were conducted on the Tecnai Model G^2F20 system (FEI Co. (America)) under an accelerating voltage of 200 kV. Scanning electron microscopy (SEM) (JEOL, Model JSM7500F) showed the morphologies of the samples. Thermogravimetric analyses were analyzed by a Netzsch Model TG 209 TG-DTA analyzer with a heating rate of 15 °C min^{-1} from 25 °C to 700 °C.

2.3. Synthesis of Eu-MOF and Tb-MOF

As reported in our previous work, the boric-acid-functional Eu-MOF was prepared via a simple solvothermal method (Wang et al., 2018a,b). $EuCl_3{\cdot}6H_2O$ (10 mmol L^{-1} or 2.5 mmol L^{-1}) and BBDC (10 mmol L^{-1} or 2.5 mmol L^{-1}) were mixed under vigorous stirring for 15 min in DMF/H_2O (7:3) solution. The mixed solution was then placed in a Teflon-lined stainless steel autoclave and heated at 120 °C for 12 h. The obtained product was cooled to room temperature, and then centrifuged and washed thoroughly with DMF and ethanol three times. The samples were dried in a vacuum oven at room temperature. Eu-MOF was displayed white powder. Tb-MOF were synthesized with the same procedure to that of Eu-MOF, except $TbCl_3{\cdot}6H_2O$ (10 mmol L^{-1}) were used as metal center.

2.4. Ratiometric detection of H_2O_2

For the detection of H_2O_2, the aqueous solution of Eu-MOF (0.05 mg mL^{-1}) was added into a 5 mL quartz cuvette. Then, the concentration-dependent fluorescence sensing investigation was accomplished by the stepwise addition (30 μL in each step) of H_2O_2 (10 μM) to the suspension of Eu-MOF (2 mL) with a final volume of 3 mL. The fluorescence spectra were recorded with excitation at 270 nm before and after the addition of H_2O_2 and were collected in range of 300–800 nm. The reaction product was collected after washed by water and ethanol three times. The samples were dried in a vacuum oven at 50 °C as white powder. Afterwards, time-dependent fluorescence studies were completed by adding 300 μL of H_2O_2 solution to the suspension of Eu-MOF until the fluorescence intensity was saturated. Tb-MOF were treated for the detection of H_2O_2 in a similar procedure to Eu-MOF, except for the use of Tb-MOF (0.05 mg mL^{-1}) as the probe. The fluorescence spectra were recorded with excitation at 270 nm. To validate the application of the detection of H_2O_2 in real sample, rainwater samples were collected without any treatment and stored at room temperature prior to analysis. The spiked samples were prepared by the addition of 10 μM H_2O_2 in rainwater.

2.5. Ratiometric detection of glucose

For the detection of glucose, 30 μL of GOx (0.2 mg mL^{-1}) was mixed with 30 μL of glucose solution with different concentrations and incubated at 37 °C for 1 h (Chang et al., 2018; Xiao et al., 2018; Chen et al., 2019). Then, the concentration-dependent fluorescence sensing investigations were accomplished by adding the mixture to the suspension of Eu-MOF (2 mL) with a final volume of 3 mL. The fluorescence spectra with excitation at 270 nm were recorded in range of 300–800 nm. For detection of glucose concentration of mouse urine, sample was collected from mice and diluted 100 times by NaAc buffer for detection.

3. Results and discussion

3.1. Preparation and characterization of Eu-MOF

Boric-acid-functional Eu-MOF was prepared with 5-boronobenzene-1,3-dicarboxylic acid (BBDC) and $EuCl_3$ via a simple solvothermal method with some alteration to our previous work (Wang et al., 2018a,b). The scanning electron microscope (SEM) image shows that the as-synthesized Eu-MOF has a uniform dispersion with an average

diameter of 2.3 μm (Fig. S1A, E). To investigate the effect of concentration of reactants, we reduce the content of $EuCl_3$ and BBDC with certain solvent. Hollow spheres with 100–150 nm were obtained when $EuCl_3{\cdot}6H_2O$ (0.025 mmol) and BBDC (0.025 mmol) were selected (Fig. S1B and S1F). Due to its larger superficial area for high efficiency, the hollow ones were chosen for the further work. The Eu-MOF was well-dispersed according to the transmission electron microscopy (TEM) images (Fig. S1C and S1D).

The powder X-ray diffraction (PXRD) patterns of Eu-MOF were recorded and agreed well with the simulated patterns of the Eu-MOF2 (Yang et al., 2017) using Eu^{3+} as the metal node and isophthalic acid as the ligand (Fig. S2). Therefore, boric group did not coordinate with Eu^{3+} ion, and as a free accessible site, the functional group was expected to approach the analytes, such as H_2O_2 in aqueous phase. The peak at 1598 and 1426 cm^{-1} in Fourier transform infrared spectra (FTIR) of Eu-MOF arises from the asymmetric and symmetric carboxylate stretching vibrations of the BBDC ligand (Fig. S3). The spectrum of both Eu-MOF and BBDC showed a band at 1315 cm^{-1} for the absorption of the B—O bond, and the result also indicated that the Eu-MOF has a free boric acid site.

3.2. Optical properties of Eu-MOF and Tb-MOF

The optical properties of Eu-MOF were investigated in detail via the analysis of UV–vis absorption and fluorescence spectra. Both the absorption spectrum of BBDC and Eu-MOF showed a significant absorption band at 260–300 nm, which resulted from the π-π* transition of BBDC (Fig. 1A). As shown in Fig. 1B, BBDC, Tb-MOF, and Eu-MOF displayed their special emissions with the single excitation at 270 nm, respectively. A strong emission at 350 nm was observed from BBDC, while the Eu-MOF had a similar band at 370 nm and owned four special peaks at 590–710 nm, which is the characteristic emission of Eu^{3+} ions. Compared with the emission of BBDC, the red-shift band at 370 nm occurred in the spectrum of Eu-MOF because the extensive π-conjugated system formed between Eu^{3+} and BBDC. As illustrated in Fig. 1C, with antenna effect procedure, BBDC absorbs photons to produce its triplet state through intersystem crossing procedure. Then the triplet state matches the energy levels of Eu^{3+} (D_0) and Tb^{3+} (D_4) to sensitize Eu^{3+} and Tb^{3+} ions. Therefore, the Ln^{3+} ions show enhanced emission compared with their free states. Table S1 listed the energy gap between T1 of BBDC and Ln^{3+} ions. Because of the big gap between T1 of the ligand and the excited state of Eu^{3+} ions, incomplete energy transfer in Eu-MOF achieved the dual emission. Moreover, all the emissions own the same source: the absorbed photons of BBDC, so they were excited at the single wavelength at 270 nm. Tb-MOF showed the characteristic emission of Tb^{3+} ions at 490–640 nm. However, the higher match degree between the excited state of Tb^{3+} and T1 of BBDC and therefore higher energy transfer resulted in efficient sensitization of Tb^{3+} ions and the less emission from BBDC. Additionally, the intensity of dual-fluorescence emission from Eu-MOF remained constant within a week (Fig. 1D). Thus, the Eu-MOF was a prospective material for sensing application because of its high chemical stability and the dual-fluorescence emission for ratiometric sensing and visual detection.

3.3. Ratiometric detection of H_2O_2

Considering the unique nucleophilic reaction between boric group and H_2O_2, the changes of the fluorescence spectra of Eu-MOF were recorded under the stepwise addition of H_2O_2. When H_2O_2 concentration increased, the emission at 354 nm was enhanced and the emission at 623 nm decreased, corresponding to the emission from BBDC and Eu^{3+}, respectively (Fig. 2A). As shown in Fig. S5, the fluorescence

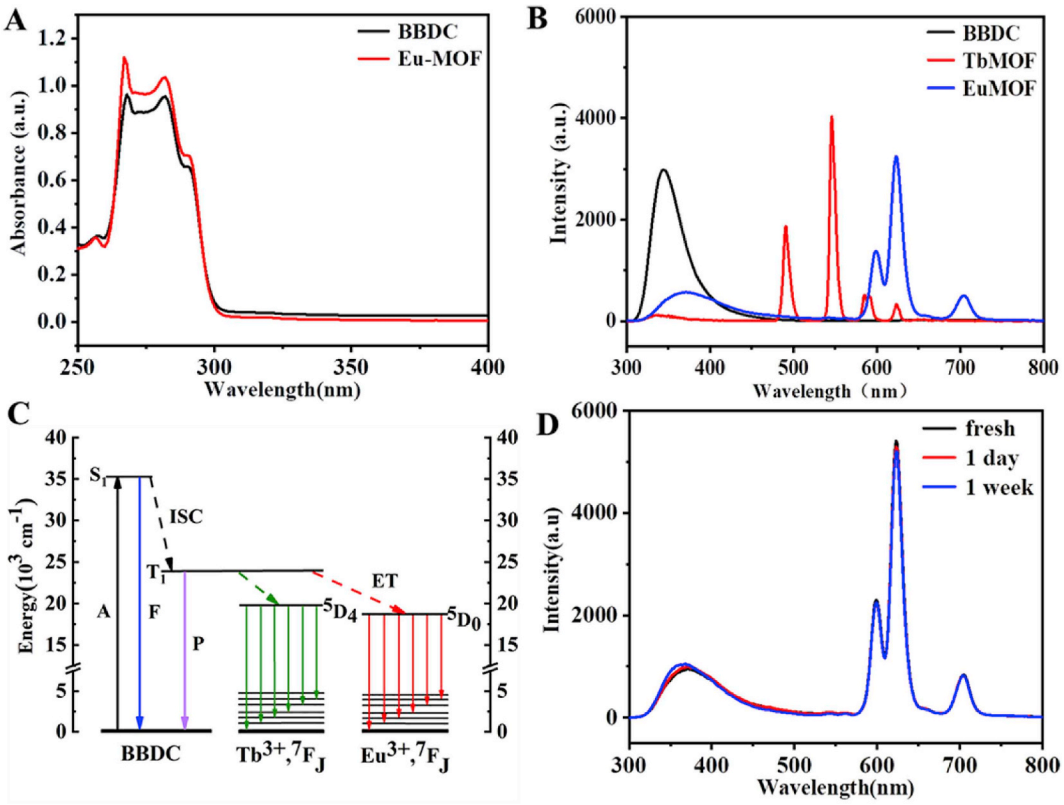

Fig. 1. (A) UV–vis spectra of BBDC and Eu-MOF in aqueous solution; (B) Emission spectra of BBDC, Eu-MOF and Tb-MOF in aqueous solution at the excitation of 270 nm; (C) Schematic illustration of the absorption, migration, and emission from Eu-MOF and Tb-MOF with antenna effect procedure, where A represents the absorption at 275 nm, F for fluorescence, P for phosphorescence. (ISC: intersystem crossing; ET: energy transfer; S: singlet; T: triplet). (D) Day-to-day fluorescence stability of 0.05 mg L^{-1} Eu-MOF aqueous solution stored in room temperature.

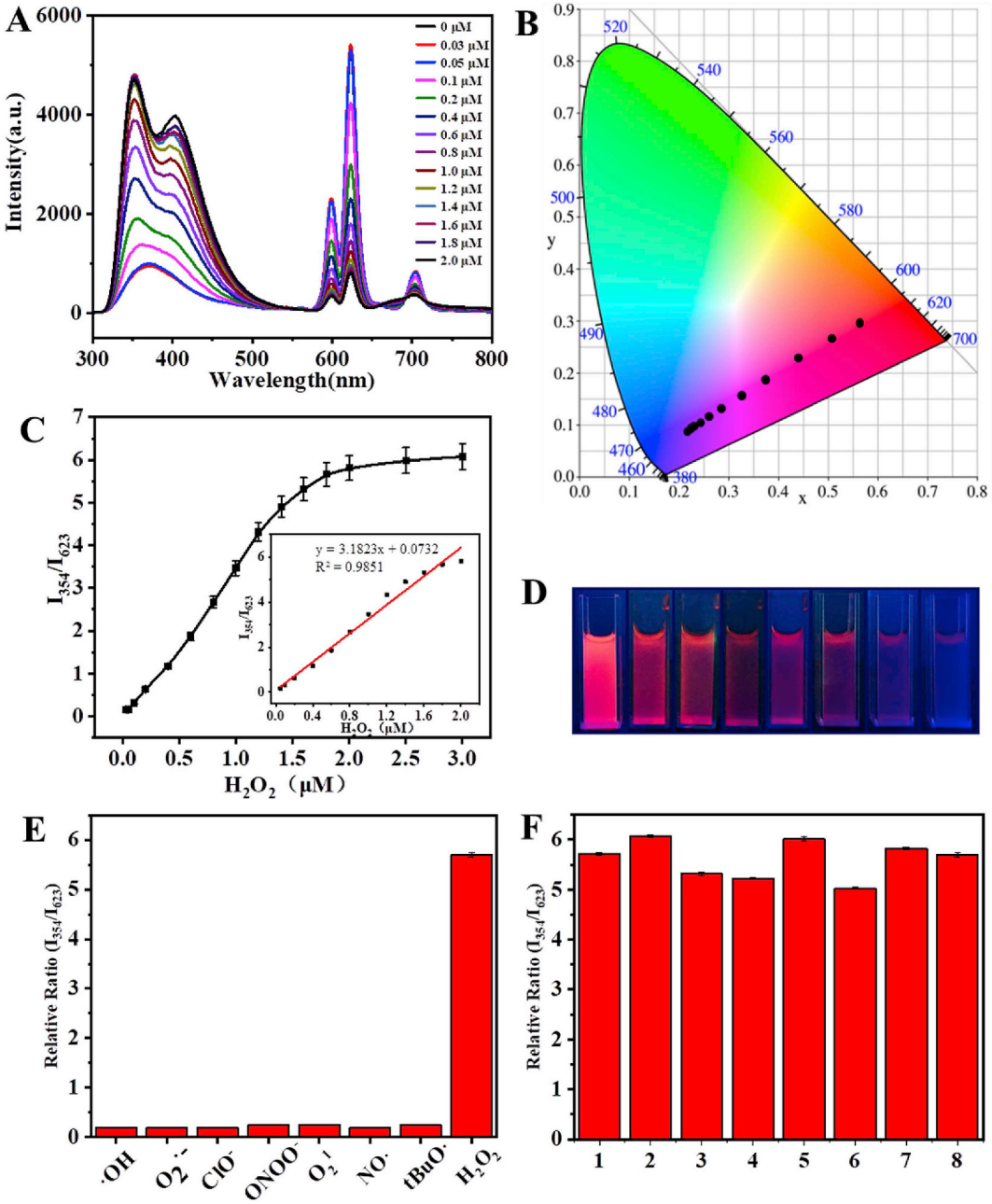

Fig. 2. (A) Fluorescence spectra of 0.05 mg mL^{-1} Eu-MOF with the stepwise addition of H_2O_2 under the single excitation at 270 nm. (B) CIE chromaticity coordinates of Eu-MOF with the addition of H_2O_2 at different concentration. (C) Plot of the intensity ratio of I_{354}/I_{623} vs H_2O_2 concentration. (D) Images of the mixture solution at different concentration of H_2O_2 under UV irradiation. (E) Comparison of fluorescence ratio of Eu-MOF in the presence of various ROS and RNS at the excitation of 270 nm; (F) Fluorescence ratio of Eu-MOF in response to 2 μM H_2O_2 and 10 μM other ROS and RNS as the interference component, (1) H_2O_2 + ·OH, (2) $H_2O_2 + O_2^-$, (3) $H_2O_2 + ClO^-$, (4) $H_2O_2 + ONOO^-$, (5) $H_2O_2 + O_2^1$, (6) H_2O_2 + NO·, (7) H_2O_2 + tBuO·, and (8) single H_2O_2.

spectra of mixed solution had a big change for the first 20 min of reaction and after that the ratio became stable. Thus, after 20 min of BBDC reaction with H_2O_2, the fluorescence spectra were recorded. The fluorescence response approved that the boric-acid-functional Eu-MOF is exactly useful for the detection of H_2O_2 by ratiometric fluorescent strategy. The fluorescence intensity of Eu-MOF was recorded after solution reacting with H_2O_2 at the concentration from 0 to 3 μM. A good linear correlation was obtained between the intensity ratio of the emission at 354 and 623 nm and H_2O_2 concentration in the range from 0.05 μM to 2 μM with a coefficient of $R^2 = 0.9851$ (Fig. 2C). The limit of detection (LOD) based on 3σ/k (where σ is the standard deviation of blank measurement, and k is the slope of calibration graph) was 0.0335 μM, which was comparable or superior to most fluorescence probes for H_2O_2 reported previously (Table S2). Ratiometric fluorescence detection of H_2O_2 was achieved with the Eu-MOF as probe.

As illustrated in Fig. 2D, when the concentration of H_2O_2 increased, strong red fluorescence diminished and changed to blue gradually. CIE chromaticity was also in accordance with the color change (Fig. 2B). The obvious color change is very useful for visual detection with naked eyes. As a contrast, H_2O_2 sensing with the Tb-MOF as probe was also tested. Unlike Eu-MOF, only did the emission of Tb-MOF at 551 nm decrease under the addition of H_2O_2 at different concentrations, corresponding to single fluorescence intensity change of green emission (Fig. S6). Compared with the single fluorescence sensors, the

ratiometric fluorescence Eu-MOF is clearly better due to the character that is easier to be differentiated by naked eye with the color change. Moreover, we investigated the fluorescence intensity change of 354 and 623 nm after the addition of H_2O_2, respectively. Neither of them had a good and simple linear relationship with the concentration of H_2O_2 (Fig. S7 and S8), but their ratio showed a linear response as illustrated in Fig. 2C. Besides, as shown in Fig. S9, the fluorescence intensity ratio of I_{370}/I_{623} remained undisturbed by different Eu-MOF concentration, so higher signal stability was obtained than the single emission probe by the built-in correction. Because of the self-reference obtained for dual emission from single probe, ratiometric fluorescence showed a high tolerance of probe concentration interference. These results demonstrated that a simple and practical detection method of H_2O_2 was realized by adopting the ratiometric fluorescence strategy based on Eu-MOF.

To evaluate the selectivity of the Eu-MOF probe to H_2O_2, the fluorescence intensity in response to various reactive oxygen species (ROS) or reactive nitrogen species (RNS) was investigated. Under the identical conditions, no significant change of the fluorescence intensity in the presence of the ROS or RNS was observed except H_2O_2 (Fig. 2E) because H_2O_2 owns the unique ambiphilic reactivity to boric group, which is different to the other species. Besides, we investigated the fluorescence change of the Eu-MOF under the addition of H_2O_2 in the presence of other species as interference. It is obvious that the other ROS or RNS did not interfere with the reaction of Eu-MOF and H_2O_2 (Fig. 2F). The result shows the Eu-MOF probe was highly selective to H_2O_2, and our strategy was effective and useful.

To investigate the practical applications of the dual-emission Eu-MOF, the detection of H_2O_2 in rainwater sample was carried out. The samples were used without any pretreatment. As shown in Table 1, no H_2O_2 was detected at the present condition. However, quantitative results in solution state exhibited the recoveries ranged from 99.5% to 103.9%, with the relative standard deviations (RSD) of below 2.7%. Thus, the Eu-MOF has good prospects for application in H_2O_2 detection.

3.4. Ratiometric detection of glucose

The ratiometric fluorescence detection platform shows a cheerful prospect for sensing H_2O_2, so the metabolites, which participate in H_2O_2 generation, is also expected to be detection with H_2O_2 as medium. Considering the enzymatic reaction between glucose and glucose oxidase (GOx) to produce H_2O_2, the capability of the Eu-MOF probe for glucose detection was also investigated. In the presence of GOx, when glucose concentration increased, the emission at 354 nm enhanced, while the emission at 623 nm decreased, corresponding to the emissions from BBDC and Eu^{3+}, respectively (Fig. 3A). The fluorescence response approved that the Eu-MOF probe is highly potential for the sensitive detection of glucose with our ratiometric fluorescent strategy exactly. The fluorescence intensity was recorded with the glucose concentration from 0 to 6 μM. A good linear correlation was obtained between the intensity ratio and glucose concentration in the range from 0.1 μM to 4 μM with a coefficient of determination of $R^2 = 0.9824$ (Fig. 3C). The LOD based on 3σ/K was 0.0643 μM, which was comparable or superior to most fluorescence probes for glucose reported previously (Table S3).

As illustrated in Fig. 3D, when the concentration of glucose increased, strong red fluorescence diminished and gradually changed to blue. The dual fluorescence probe was easily differentiated by the naked eye and showed a high tolerance of concentration interference. CIE chromaticity coordination confirmed the color changes (Fig. 3B). The results demonstrated that a simple and practical detection method of glucose was realized by adopting our ratiometric fluorescence strategy with dual-emission Eu-MOF as probe.

To evaluate the selectivity of the Eu-MOF probe to glucose, fluorescence intensity in response to various saccharides and amino acids was investigated. Under the identical conditions, no significant changes of the fluorescence intensity in the presence of saccharides and amino acids were found except glucose (Fig. 3E) because of the high selective catalysis of glucose with GOx. We also investigated the fluorescence change of the Eu-MOF under the addition of glucose with other materials as interference. It is obvious that other materials have little interference with the reaction of Eu-MOF and glucose (Fig. 3F). As neutral saccharides can coordinate with boric acid (Li et al., 2015), the direct fluorescence response of the Eu-MOF to glucose was also tested. However, a low sensitivity was observed because of the lack of sufficient electronic change in either the boric acid or the saccharide moiety (Fig. S10). The result shows our sensing system containing the Eu-MOF and GOx was highly selective and sensitive to glucose. Our strategy was proved feasible.

To investigate the real sample applications of the dual-emission Eu-MOF, glucose in mouse urine samples was detected. No glucose was detected from the sample. The recovery experiment was carried out after glucose standard solution with different concentrations was added to the urine samples before dilution. Table 2 shows the quantitative results in solution state, and the recoveries ranging from 97.6% to 102.2% were obtained, with all the relative standard deviations (RSD) below 3.0%, indicating that the Eu-MOF has good prospects for application in glucose detection.

Table 1
Results of H_2O_2 detection in rainwater (n = 3).

Sample	Added (μM)	Found (μM)	Recovery (%)	RSD (%)
1	0	ND[a]		
2	0.05	0.05196	103.9	1.3
3	0.2	0.2077	103.8	2.7
4	0.5	0.5092	101.8	1.0
5	1.0	0.9947	99.5	1.3
6	1.5	1.526	101.7	1.6

[a] ND, not detected.

3.5. Mechanisms of H_2O_2 and glucose detection

It is well known that H_2O_2 possesses ambiphilic reactivity, which is different obviously from other biological ROS such as $^1O_2$, ·OH, HClO (Li et al., 2015). H_2O_2 is two-electron electrophilic because of its unstable O—O bond. Moreover, H_2O_2 is also an excellent nucleophile with the existence of α-effect of adjacent nonbonding orbitals on its oxygen atoms (Lippert et al., 2011). Considering that aryl boronate are complementary to H_2O_2 through ambiphilic reactivity, BBDC is selected to design our H_2O_2 sensing platform.

As shown in Scheme 1, the dual emission from Eu-MOF is the result of the antenna effect and incomplete energy transfer caused by energy gap between the excited state of Eu^{3+} ions and the triplet state of BBDC. In the presence of H_2O_2, boric acid group forms a negatively charged tetrahedral boronate complex with nucleophilic H_2O_2 with nucleophile reaction. The boric acid group then cracked to become hydroxyl group as reported previously (Gough and Cotter, 2011). After boric acid group becomes hydroxyl group, the intersystem crossing efficiency for the sensitization Eu^{3+} ions decreases.

To validate the proposed mechanism, the emissive behavior of Eu-MOF before and after the addition of H_2O_2 was recorded. Dual emission at 370 nm from BBDC and 623 nm from Eu^{3+} was observed. After the addition of H_2O_2, the emission at 354 nm enhanced, while the emission at 623 nm decreased because of the decreased intersystem crossing efficiency. The fluorescence profile of the mixture of Eu^{3+} and 5-hydroxyisophthalic acid (5-hisp) was recorded in Fig. S11. The fluorescence of Eu-MOF after the addition of H_2O_2 was similar to that obtained from Eu^{3+} and 5-hisp. Moreover, different powder X-ray diffraction (PXRD) patterns of Eu-MOF were observed before and after the addition of H_2O_2 (Fig. S2), indicating the structural change of Eu-MOF after reacted with H_2O_2. The peak at 1315 cm^{-1} of the B—O bond of Eu-MOF

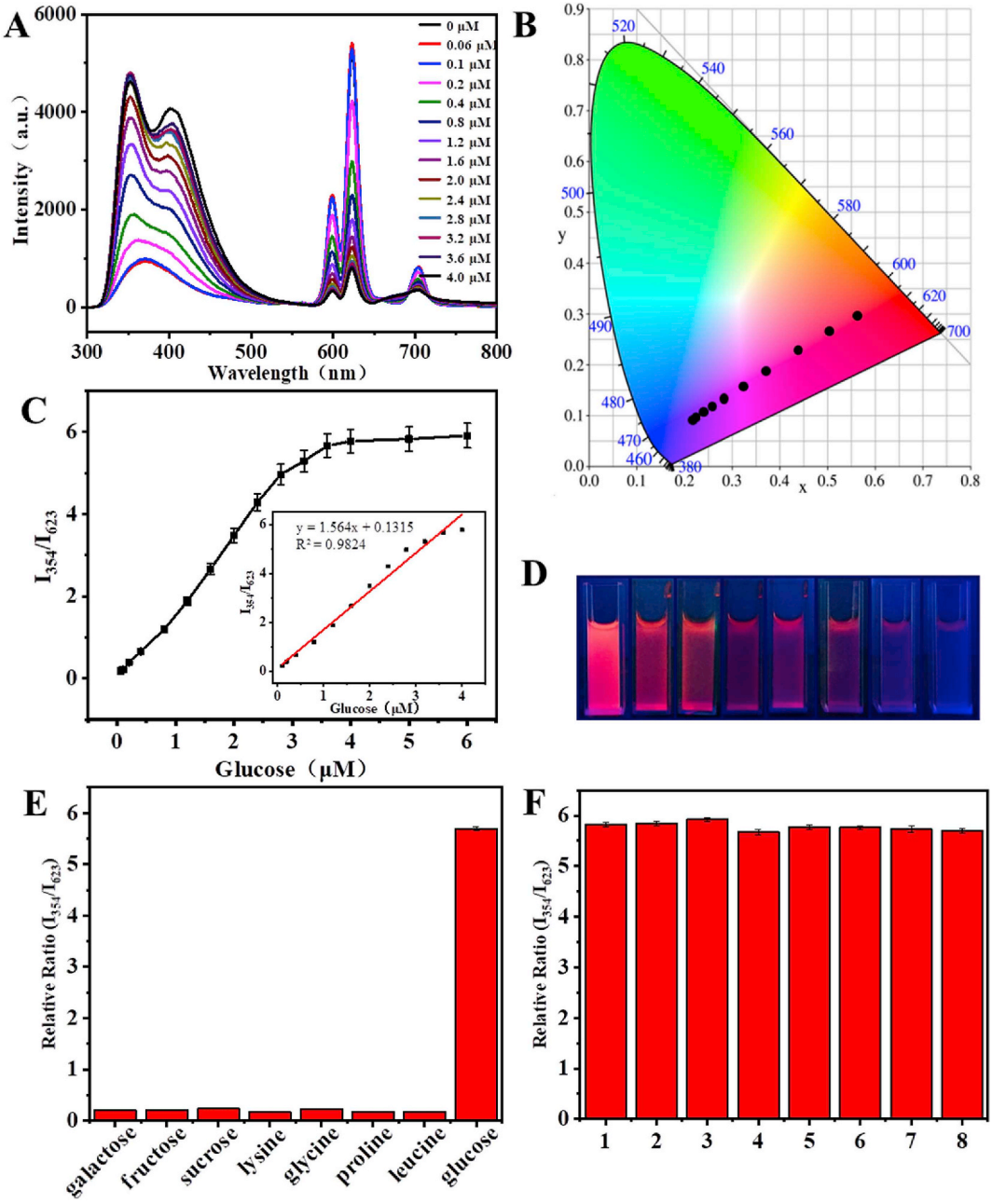

Fig. 3. (A) Fluorescence spectra of reaction solution with the addition of glucose at different concentration under the excitation of 270 nm. (B) CIE chromaticity coordinates of reaction solution with the addition of glucose at different concentration. (C) Plot of the intensity ratio of I_{354}/I_{623} vs glucose concentration under UV irradiation. (D) Images of the mixture solution at different concentration of glucose. (E) Comparison of fluorescence ratio of Eu-MOF in the presence of other biologically relevant species at the excitation of 270 nm. (F) Fluorescence ratio of Eu-MOF in response to 4 μM glucose and 20 μM other biologically relevant species as the interference, (1) glucose + galactose, (2) glucose + fructose, (3) glucose + sucrose, (4) glucose + lysine, (5) glucose + glysine, (6) glucose + proline, (7) glucose + leucine, (8) glucose.

Table 2
Results of glucose detection in mouse urine (n = 3).

Sample	Added (μM)	Found (μM)	Recovery (%)	RSD (%)
1	0	ND[a]		
2	0.1	0.09757	97.6	2.0
3	0.4	0.3962	99.1	2.3
4	1.0	1.017	101.7	1.3
5	2.0	2.045	102.2	1.1
6	3.0	2.946	98.2	3.0

[a] ND, not detected.

disappeared from the Fourier transform infrared spectra (FTIR), when the peaks at 3388 and 1181 cm^{-1} of phenol hydroxyl were observed after reacted with H_2O_2 (Fig. S12). The FTIR result provided the direct evidence for the change from boric group to hydroxyl group. Thus, the ratiometric fluorescence platform was successfully established.

Glucose can coordinate with boric acid group via covalent interactions in aqueous solution. However, the design of glucose sensor based on boric acid functional MOF is always failed due to the lack of sufficient electronic changes. H_2O_2 is the production from glucose reaction with its specific oxidoreductases GOx and O_2. Different to strategy based on boric acid-glucose interaction with weak change, the Eu-MOF

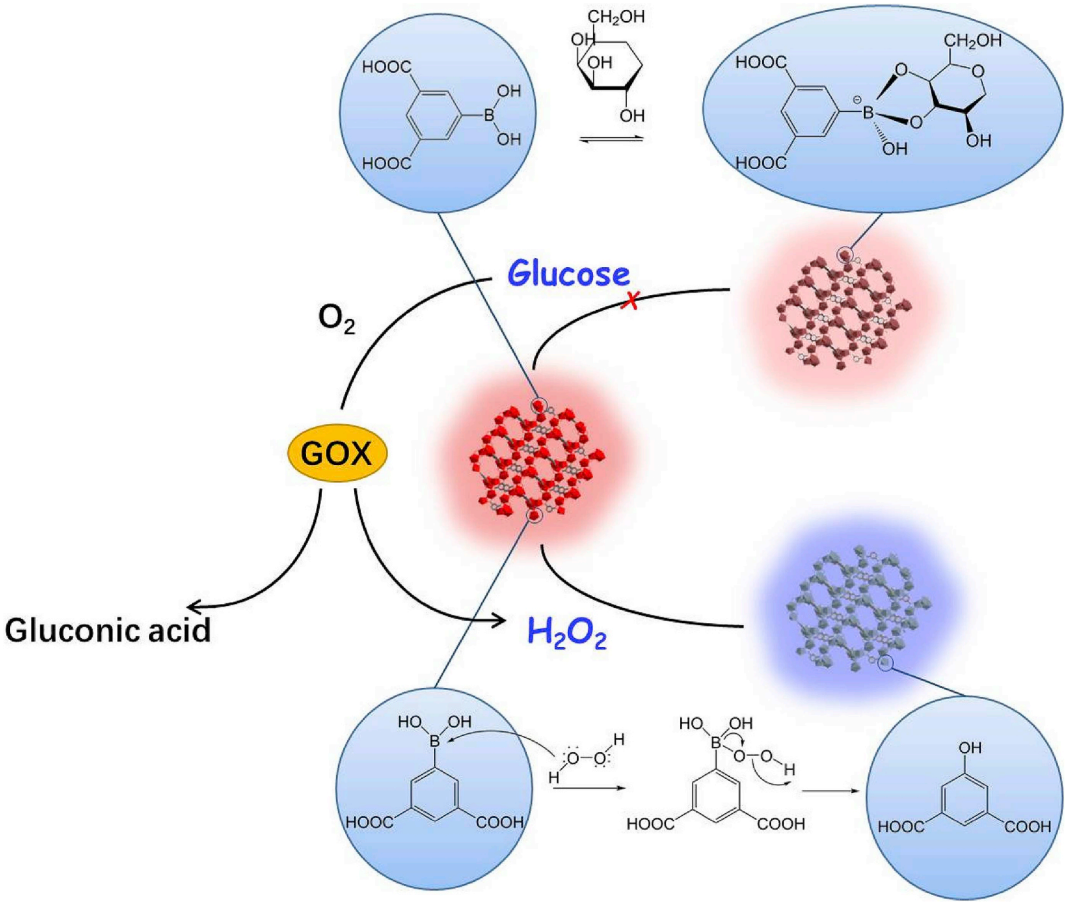

Scheme 1. Proposed mechanism for fluorescence behavior of Eu-MOF in presence of H_2O_2 or glucose.

and GOx sensing system showed a great color change after glucose was added for the generation of H_2O_2 with the mechanism illustrated in Scheme 1. Our detection strategy adding GOx and basing on H_2O_2 reactions completely solved the problem that the reversible covalent interactions of boric acid group could not be used for detecting glucose. Although the reaction of BBDC with H_2O_2 is irreversible and the material cannot be recycled, Eu-MOF has virtues, such as inexpensive, simple procedure and long-term storage stability. The aforementioned results clearly demonstrated the feasibility of the ratiometric fluorescence detection strategy for H_2O_2 and glucose based on boric-acid-functional Eu-MOF.

4. Conclusions

In summary, we have fabricated the boric acid-functional Eu-MOF via a simple one-pot solvothermal method for the detection of H_2O_2 and glucose. By simply decorated with the boric acid group for the ligand, the functional Eu-MOF exhibited dual-emission at a single excitation and was ready to use for ratiometric fluorescent detection through the ambiphilic reaction between boric acid group and H_2O_2. While the special reaction achieves high selectivity, the reaction is also used to tune the energy transfer efficiency for the ratiometric fluorescence sensing and visual detection. Compared with the single fluorescence sensors, nanometer sphere Eu-MOF displayed a more obvious color change for visual detection of H_2O_2. The ratiometric fluorescence platform for H_2O_2 and glucose was successfully developed with LOD of 0.0335 and 0.0643 μM, respectively. The proposed strategy was simple, intuitive, highly sensitive and selective. Thus, it is possible to be further expanded to detect other metabolites involved in H_2O_2-generating reaction in future.

Declaration of interests

The authors declare that they have no known competing financial interests or personal relationships that could have appeared to influence the work reported in this paper.

Conflict of interest

All authors declare no conflict of interest.

CRediT authorship contribution statement

Yu Cui: Methodology, Formal analysis, Writing - original draft, Writing - review & editing. **Fei Chen:** Methodology, Formal analysis. **Xue-Bo Yin:** Project administration, Supervision, Writing - review & editing.

Acknowledgements

This work was supported by National Natural Science Foundation of China (Grant No 21675090, 21874074, and 21435001).

Appendix A. Supplementary data

Supplementary data to this article can be found online at https://doi.org/10.1016/j.bios.2019.04.008.

References

Carroll, V., Michel, B.W., Blecha, J., VanBrocklin, H., Keshari, K., Wilson, D., Chang, C.J., 2014. J. Am. Chem. Soc. 136, 14742–14745.

Chang, J.F., Li, H.Y., Hou, T., Duan, W.N., Li, F., 2018. Biosens. Bioelectron. 104, 152–157.
Chang, K.W., Liu, Z.H., Fang, X.F., Chen, H.B., Men, X.J., Yuan, Y., Sun, K., Zhang, X.J., Yuan, Z., Wu, C.F., 2017. Nano Lett. 17, 4323–4329.
Chen, J.Q., Xue, S.F., Chen, Z.H., Zhang, S.Q., Shi, G.Y., Zhang, M., 2018. Biosens. Bioelectron. 100, 526–532.
Chen, Z.H., Han, X.Y., Deng, L.X., Lin, Z.Y., Mu, F.Y., Zhang, S., Shi, G., Zhang, M., 2019. Talanta 191, 235–240.
Cowan, E.A., Taylor, J.L., Oldham, C.D., Dasari, M., Doyle, D., Murthy, N., May, S.W., 2013. Enzym. Microb. Technol. 53, 373.
Cui, Y.J., Yue, Y.F., Qian, G.D., Chen, B.L., 2012. Chem. Rev. 112, 1126–1162.
Dickinson, B.C., Chang, C.J., 2008. J. Am. Chem. Soc. 130, 9638–9639.
Dong, Y.Q., Cai, J.H., Fang, Q.Q., You, X., Chi, Y.W., 2016. Anal. Chem. 88, 1748–1752.
Fang, Y., Tan, J.J., Choi, H., Lim, S., Kim, D.H., 2018. Sens. Actuators, B 259, 155–161.
Foreman, J., Demidchik, V., Bothwell, J.H.F., Mylona, P., Miedema, H., Torres, M.A., Linstead, P., Costa, S., Browniee, C., Jones, J.D.G., 2003. Nature 422, 442–446.
Furukawa, H., Cordova, K.E., O'Keeffe, M., Yaghi, O.M., 2013. Science 341, 1230444.
Gallis, D.F.S., Rohwer, L.E.S., Rodriguez, M.A., Barnhart, M.C., Butler, K.S., Luk, T.S., Timlin, J.A., Chapman, K.W., 2017. ACS Appl. Mater. Interfaces 9, 22268–22277.
Gough, D., Cotter, T., 2011. Cell Death Dis. 2, e213.
Hansson, G.K., Libby, P., 2006. Immunology 6, 508–519.
Hu, Z.C., Deibert, B.J., Li, J., 2014. Chem. Soc. Rev. 43, 5815–5840.
James, T.D., Sandanayake, K.R.A.S., Iguchi, R., Shinkai, S., 1995. J. Am. Chem. Soc. 117, 8982–8987.
Jia, P.L., Zhou, Y.P., Zhang, X.F., Zhang, Y.R., Dai, H., 2018. Water Res. 131, 122–130.
Jiang, Y.Y., Ni, P.J., Chen, C.X., Lu, Y.Z., Yang, P., Kong, B., Fisher, A., Wang, X., 2018. Adv. Energy Mater. 8, 1801909.
Lee, M.H., Kim, J.S., Sessler, J.L., 2015. Chem. Soc. Rev. 44, 4185–4191.
Li, D.J., Chen, Y., Liu, Z., 2015. Chem. Soc. Rev. 44, 8097–8123.
Lin, M.T., Beal, M.F., 2006. Nature 443, 787–795.
Lippert, A.R., Bittner, G.C.V.D., Chang, C.J., 2011. Acc. Chem. Res. 44, 793–804.
Liu, W., Huang, X., Xu, C., Chen, C., Yang, L., Dou, W., Chen, W., Yang, H., Liu, W., 2016. Chem. Eur J. 22, 18769–18776.
Nosaka, Y., Nosaka, A.Y., 2017. Chem. Rev. 117, 11302–11336.
Paulsen, C.E., Carroll, K.S., 2013. Chem. Rev. 113, 4633.
Peng, C., Zhou, S.Y., Zhang, X.M., Zeng, T.Q., Zhang, W., Li, H.M., Liu, X.Y., Zhao, P., 2018. Sens. Actuators, B 270, 530–537.
Srikun, D., Albers, A.E., Chang, C.J., 2011. Chem. Sci. 2, 1156–1165.
Sun, X.L., Xu, S.Y., Flower, S.E., Fossey, J.S., Qian, X.H., James, T.D., 2013. Chem. Commun. 49, 8311–8313.
Sun, Z., Li, Y.G., Ma, Y., Li, L.C., 2017. Dyes Pigments 146, 263–271.
Van de Bittner, G.C., Dubikovskaya, E.A., Bertozzi, C.R., 2010. Proc. Natl. Acad. Sci. U.S.A. 107, 21316–21321.
Wang, Y.M., Tian, X.T., Zhang, H., Yang, Z.R., Yin, X.B., 2018a. ACS Appl. Mater. Interfaces 10, 22445–22452.
Wang, Y.M., Yang, Z.R., Xiao, L.H., Yin, X.B., 2018b. Anal. Chem. 90, 5758–5763.
Xiao, N., Liu, S.G., Mo, S., Yang, Y.Z., Han, L., Ju, Y.J., Li, N.B., Luo, H.Q., 2018. Sens. Actuators, B 273, 1735–1743.
Xue, S.F., Han, X.Y., Chen, Z.H., Yan, Q., Lin, Z.Y., Zhang, M., Shi, G., 2018. Anal. Chem. 90, 10614–10620.
Yaghi, O.M., O'Keeffe, M., Ockwig, N.W., Chae, H.K., Eddaoudi, M., Kim, J., 2003. Nature 423, 705–714.
Yan, B., 2017. Acc. Chem. Res. 50, 2789–2798.
Yang, Z.R., Wang, M.M., Wang, X.S., Yin, X.B., 2017. Anal. Chem. 89, 1930–1936.
Zhang, M.H., Wang, D.Y., Geng, Z.M., Li, P.P., Sun, Z.L., Xu, W.M., 2018a. Food Chem. 240, 642–647.
Zhang, Q.H., Wang, J., Kirillov, A.M., Dou, W., Xu, C., Xu, C.L., Yang, L.Z., Fang, R., Liu, W.S., 2018b. ACS Appl. Mater. Interfaces 10, 23976–23986.
Zhang, T.T., Gu, Y., Li, C., Yan, X.Y., Lu, N.N., Liu, H., Zhang, Z.Q., Zhang, H., 2017. ACS Appl. Mater. Interfaces 9, 37991–37999.
Zhou, J.M., Shi, W., Li, H.M., Li, H., Cheng, P., 2014. J. Phys. Chem. C 118, 416–426.
Zhu, H., Yan, S.C., Li, Z.S., Zou, Z.G., 2017. ACS Appl. Mater. Interfaces 9, 33887–33895.